$\mathcal{O}$-GNN: INCORPORATING RING PRIORS INTO MOLECULAR MODELING

Anonymous authors
Paper under double-blind review

ABSTRACT

Cyclic compounds that contain at least one ring play an important role in drug design. Despite the recent success of molecular modeling with graph neural networks (GNNs), few models explicitly take rings in compounds into consideration, consequently limiting the expressiveness of the models. In this work, we design a new variant of GNN, ring-enhanced GNN ($\mathcal{O}$-GNN), that explicitly models rings in addition to atoms and bonds in compounds. In $\mathcal{O}$-GNN, each ring is represented by a latent vector, which contributes to and is iteratively updated by atom and bond representations. Theoretical analysis shows that $\mathcal{O}$-GNN is able to distinguish two isomorphic subgraphs lying on different rings using only one layer while conventional graph convolutional neural networks require multiple layers to distinguish, demonstrating that $\mathcal{O}$-GNN is more expressive. Through experiments, $\mathcal{O}$-GNN shows good performance on **11** public datasets. In particular, it achieves state-of-the-art validation result on the PCQM4Mv1 benchmark (outperforming the previous KDDCup champion solution) and the drug-drug interaction prediction task on DrugBank. Furthermore, $\mathcal{O}$-GNN outperforms strong baselines (without modeling rings) on the molecular property prediction and retrosynthesis prediction tasks.[1]

1 INTRODUCTION

Cyclic compounds, which refers to the molecules that have at least one ring in its system, naturally exist in the chemical space. According to our statistics on $109M$ compounds from PubChem (Kim et al., 2019) which is a widely used chemical library, more than 90% compounds have at least one ring. The rings could be small/simple (*e.g.*, the benzene is a six-member carbon ring, and the pentazole is a five-member nitrogen ring) or large/complex (*e.g.*, the molecule shown in Figure 1). Rings are important in drug discovery, for example: (1) Rings can potentially reduce the flexiblity of molecules, reduce the uncertainty when interacting with target proteins, and lock the molecules to their bioactive conformation (Sun et al., 2012). (2) Macrocyclic compounds, which usually have a ring with more than 12 atoms, play important roles in antibotics design (Venugopal & Johnson, 2011) and peptide drug design (Bhardwaj et al., 2022).

Recently, deep neural networks, especially graph neural networks (denoted as GNN) (Kipf & Welling, 2017; Hamilton et al., 2017a), have been widely used in molecular modeling. GNN takes a graph as input, and messages of different nodes are passed along edges. GNN has made great success in scientific discovery: (1) Stokes et al. (2020) train a GNN to predict growth inhibition of Escherichia coli and find that Halicin is a broad-spectrum bactericidal antibiotic. (2) Shan et al. (2022) leverage GNN to model the interactions between proteins, and they eventually obtain possible antibodies for SARS-CoV-2. In addition, GNN is widely used in drug property prediction (Rong et al., 2020a), drug-target interaction modeling (Torng & Altman, 2019), retrosynthesis (Chen & Jung, 2021), etc. However, none of the above work explicitly models the ring information into the GNNs. From the application's perspective, they miss an important feature for their tasks. From the machine learning's perspective, Loukas (2020) points that existing message-passing-based GNNs cannot properly capture the ring information when the product of network width and height are not large enough (see the Table 1 in Loukas (2020)). Therefore, with the classic GNNs, the ring information in compounds are not well leveraged.

[1]Our code is released at the anonymous GitHub repository `https://github.com/O-GNN/O-GNN`.

To tackle this issue, in this work, we propose a new model, ring-enhanced GNN (denoted as $\mathcal{O}$-GNN), that explicitly models the ring information in a compound. The $\mathcal{O}$ standards for the rings in molecules and is pronunciated as "O". Generally speaking, $\mathcal{O}$-GNN stacks L layers, and each layer sequentially updates edge representations, node representations and ring representations by aggregating their neighbourhood information. We mainly use a self-attention layer for adaptive message passing, and use a feed-forward layer to introduce non-linearity to representations.

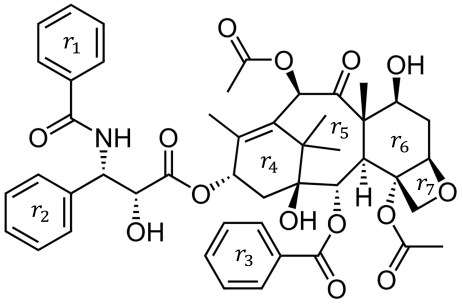

Figure 1: Paclitaxel, a compound with 7 simple rings. Kampan et al. (2015) summarized that the intact taxane ring (i.e., r_4, r_5, r_6) and a four-membered oxetane side ring (i.e., r_7) is essential to induce cytotoxic activity.

We first demonstrate the advantage of $\mathcal{O}$-GNN through theoretical analysis. $\mathcal{O}$-GNN is able to distinguish two isomorphic sub-graphs lying on different rings using only one layer. On the contrary, if we remove the ring-modeling components from $\mathcal{O}$-GNN, such a distinguishability will require multiple layers (see Section 3.2 for the detailed analysis). These results demonstrate that $\mathcal{O}$-GNN is more expressive than conventional graph convolutional networks without explicitly modeling rings.

We then conduct experiments on 11 datasets from three tasks, including molecular property prediction, drug-drug interaction prediction and retrosynthesis.

(1) For molecular property prediction, we first conduct experiments on PCQM4Mv1, which is to predict the HOMO-LUMO gap of a molecule. Our method outperforms the champion solution of KDDCup on the validation set (Shi et al., 2022) (note that test set labels are not available). Next, we verify $\mathcal{O}$-GNN on six datasets from MoleculeNet (Wu et al., 2018), which is to predict several pharmaceutical related properties of molecules. $\mathcal{O}$-GNN outperforms the corresponding GNN baselines without rings. Finally, we conduct experiments on FS-Mol (Stanley et al., 2021), a few-shot property prediction task, and shows that modeling rings can also improve the prediction accuracy.

(2) For drug-drug interaction prediction, which is to predict whether two drugs interacts with each other, we test $\mathcal{O}$-GNN on DrugBank following the previous settings (Nyamabo et al., 2021; Li et al., 2022), and achieve state-of-the-art results.

(3) For retrosynthesis, we apply $\mathcal{O}$-GNN to LocalRetro (Chen & Jung, 2021), a strong GNN-based method for retrosynthesis. On USPTO-50k, our method significantly boosts the accuracy.

2 BACKGROUND AND PRELIMINARY

In this section, we briefly introduce the background of graph neural networks.

Notations: Let $G = (V, E)$ denote a molecular graph, where V and E are the collections of nodes/atoms and edges/bonds[2]. Let R denote the collection of rings in G. Define $V = \{v_1, v_2, \cdots, v_{|V|}\}$ and $E = \{e_{ij}\}$, where v_i is the i-th atom and e_{ij} is the bond connecting v_i and v_j. When the context is clear, we use i to denote atom v_i, and use $e(v_i, v_j)$ to denote edge e_{ij}. Let $\mathcal{N}(i)$ denote the neighbors of atom i, i.e., $\mathcal{N}(i) = \{v_j \mid e_{ij} \in E\}$. Define $R = \{r_1, r_2, \cdots, r_{|R|}\}$, where each r_i is a simple ring. A simple ring does not contain any ring structure. For example, for the molecule in Figure 2, it has two simple rings as we marked (r_1 and r_2). The ring $(1, 2, 3, 4, 5, 6, 7, 8, 9, 1)$ is not a simple ring. Let $R(v_i)$ and $R(e_{ij})$ denote the rings that the atom v_i or the bond e_{ij} lies on, and $V(r)$ and $E(r)$ denote all the atoms and the bonds lying on ring r. For example, in Figure 2, $R(v_4) = \{r_1, r_2\}$ while $R(v_3) = r_2$. $R(e_{49}) = \{r_1, r_2\}$ while $R(e_{78}) = r_1$. $V(r_1) = \{v_4, v_5, v_6, v_7, v_8, v_9\}$ and $E(r_1) = \{e_{45}, e_{56}, e_{67}, e_{78}, e_{89}, e_{94}\}$.

[2]When the context is clear, we use nodes/atoms and edges/bonds alternatively in this work.

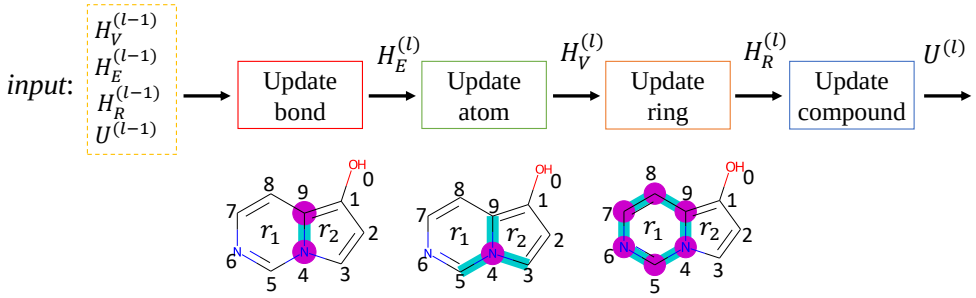

Figure 2: The workflow of our method. $H_E^{(l)}$, $H_V^{(l)}$, $H_R^{(l)}$ and $U^{(l)}$ denote the representation collections of bond, atom, ring and the global compound at the l-th layer.

A graph neural network (GNN) is usually stacked by several identical GNN layers. Each GNN layer is composed of an Aggregate function and an Update function,

$$h_i' = \text{Update}\left(h_i, \text{Aggregate}(h_j | j \in \mathcal{N}(i))\right), \tag{1}$$

where h_i is the representation of atom i and h_i' is its updated representation. Different GNNs have different Aggregate functions which determine how to aggregate information from neighbors and Update functions which determine how to update hidden states according to its aggregated information. GCN (Kipf & Welling, 2017) aggregates its neighbor information according to the adjacency matrix and degree matrix, and then updates the aggregated information with a linear transformation and a non-linear activation layer. GraphSAGE (Hamilton et al., 2017b) aggregates the neighbors information by element-wise average. GAT (Veličković et al., 2017) introduces the attention mechanism into GNN, by which it can adaptively aggregates the representations of the neighbors. Brody et al. (2021) propose the GATv2 to improve the attention mechanism in a more expressive way. Xu et al. (2018) develop a simple aggregate function which involves an ϵ parameter and multi-layer perceptrons (MLPs) which is provably as powerful as the Weisfeiler-Lehman graph isomorphism test. Besides, Gilmer et al. (2017b); Li et al. (2017); Pham et al. (2017) propose to augment the graph with a virtual node to capture the global information of the graph. A virtual node connects to all the other nodes in the graph and is jointly updated during training. Its effectiveness is validated in a series of graph classification tasks.

However, these work do not explicitly use the ring R in graph neural networks. Complementary to these work, we consider how to incorporate the ring information, which is another important component on top of the node and edge information, into molecular modeling. These advanced Aggregate and Update functions are also applicable to our work.

3 METHOD

In this section, we first introduce our model in detail and then theoretically analyze the better expressiveness of our model against traditional GNNs.

3.1 MODEL

Our model consists of L identical layers with different parameters. The architecture of each layer is shown in Figure 2. Let $h_i^{(l)}$, $h_{ij}^{(l)}$ and $h_r^{(l)}$ denote the output representations of atom v_i, bond e_{ij} and ring r at the l-th layer, respectively. Let $U^{(l)}$ denote the compound representation at the l-th layer. We initlaize $h_i^{(0)}$ via a learnable embedding layer which indicates its atomic type, chirality, degree number, formal charge, hybridization type, and so on. Similarly, we initialize $h_{ij}^{(0)}$ with a learnable embedding wich indicates its bond type, stereoisomerism type and whether the bond is conjugated. Then we initialize $h_r^{(0)}$ by concatenating the node and edge embedding and then transform it with a non-linear layer. Last, we initialize the compound representation with a learnable embedding. In

each layer, we update representations of nodes, bonds, rings and the compound sequentially. We will frequently use $\texttt{MLP}(\cdots)$, a multi-layer perception network with one hidden layer, to build our model. The inputs of $\texttt{MLP}$ are concatenated as a long vector and processed by the network.

(1) *Update bond representations*: The representation of a bond is updated via the connected atoms, the rings that the bond belongs to and the compound representation from the last layer. Mathematically,

$$h_{ij}^{(l)} = h_{ij}^{(l-1)} + \texttt{MLP}\left(h_i^{(l-1)}, h_j^{(l-1)}, h_{ij}^{(l-1)}, \frac{\sum_{r\in R(e_{ij})} h_r^{(l-1)}}{|R(e_{ij})|}, U^{(l-1)}\right). \tag{2}$$

(2) *Update atom representations*: We use an attention model to adaptively aggregate bond representations into the centralized atoms. Mathematically,

$$\begin{aligned}
&\bar{h}_i^{(l)} = \sum_{j\in\mathcal{N}(i)} \alpha_j W_v \texttt{concat}(h_{ij}^{(l)}, h_j^{(l-1)});\\
&\alpha_j \propto \exp(\boldsymbol{a}^\top \texttt{LeakyReLU}(W_q h_i^{(l-1)} + W_k \texttt{concat}(h_j^{(l-1)}, h_{ij}^{(l)})));\\
&h_i^{(l)} = h_i^{(l-1)} + \texttt{MLP}\Big(h_i^{(l-1)}, \bar{h}_i^{(l)}, \frac{1}{|R(v_i)|}\sum_{r\in R(v_i)} h_r^{(l-1)}, U^{(l-1)}\Big).
\end{aligned} \tag{3}$$

In Eqn.(3), the W's are the parameters to be learned, and $\texttt{concat}$ denotes concatenating the input vectors as a long one.

(3) *Update ring representations*: The ring representations are updated using simple feed-forward networks:

$$h_r^{(l)} = \texttt{MLP}\Big(h_r^{(l-1)}, \sum_{v_i\in V(r)} h_i^{(l)}, \sum_{e_{ij}\in E(r)} h_{ij}^{(l)}, U^{(l-1)}\Big) \tag{4}$$

(4) *Update the compound representation*:

$$U^{(l)} = U^{(l-1)} + \texttt{MLP}\left(\frac{1}{|V|}\sum_{i=1}^{|V|} h_i^{(l)}, \frac{1}{|E|}\sum_{i,j} h_{ij}^{(l)}, \frac{1}{|R|}\sum_{r\in R} h_r^{(l)}, U^{(l-1)}\right). \tag{5}$$

After stacking L $\mathcal{O}$-GNN layers, we get the graph representation by a simple average pooling layer, i.e., $h_{\mathcal{G}} = \frac{1}{|V|}\sum_{i=1}^{|V|} h_i^{(L)}$, which could be utilized by graph classification tasks. For node classification tasks, we can add a classification head to $h_i^{(L)}$.

3.2 Theoretical analysis

In this section, we compare the distinguishability between standard GNN (without ring representations) and $\mathcal{O}$-GNN. In addition to the notations defined in Section 2, we define the valued version of a graph $G = (V, E)$ as a triplet $\mathrm{VALUE}_f(G) = (V, E, f)$, where f is a mapping storing feature information and mapping a node or an edge to its corresponding input feature (e.g., a 256-dimension representation). We call f as a feature mapping on G.

Definition 1 (k-neighbourhood node)**.** *For a molecular graph $G = (V, E)$ and two nodes $u, v \in V$, we say u is a k-neighbourhood of v if there exists a path in G connecting u and v with length no larger than k. More formally, u is a k-neighbourhood of v if and only if there exists a set of nodes $\{v_0, v_1, \cdots, v_t\} \subset V$, such that, $t \le k$, $v_0 = v$, $v_t = u$, and for any $i \in \{0, \cdots, t-1\}$, $v_{i+1} \in N(v_i)$.*

We highlight here that v is a 0-neighbourhood node (and thus a k-neighbourhood node with any $k \ge 0$) of itself.

Definition 2 (k-neighbourhood sub-graph)**.** *For a molecular graph $G = (V, E)$ and a node v in G, we define the k-neighbourhood sub-graph of v as the sub-graph composed of all v's k-neighbourhood node. More formally, we slightly abuse the notations and denote the k-neighbourhood sub-graph of v as $G(v, k) \triangleq (V(v, k), E(v, k))$, where*

$$\begin{aligned}
V(v,k) &\triangleq \{u \in V :\ u \textit{ is a } k\textit{-neighbourhood node of } v\},\\
E(v,k) &\triangleq \{e(v_1, v_2) \in E : v_1, v_2 \in V(v,k)\}.
\end{aligned}$$

Definition 3 (Equivalent valued graph)**.** *For two valued graphs* $\mathrm{VALUE}_{f_1}(G_1) = (V_1, E_1, f_1)$ *and* $\mathrm{VALUE}_{f_2}(G_2) = (V_2, E_2, f_2)$*, we say that they are equivalent if (i).* G_1 *and* G_2 *are isomorphic, i.e., there exists a one-to-one mapping* $\mathcal{P} : V_1 \to V_2$*, such that the edges are preserved; (ii).* $\mathcal{P}$ *also preserves the value of edges and the the value of nodes, i.e.,* $\forall u, v \in G_1$*,*

$$e(u, v) \in E_1 \Leftrightarrow e(\mathcal{P}(u), \mathcal{P}(v)) \in E_2,$$
$$f_1(u) = f_2(\mathcal{P}(u)), f_1(v) = f_2(\mathcal{P}(v)), f_1(e(u, v)) = f_2(e(\mathcal{P}(u), \mathcal{P}(v))).$$

With all the preparations above, we are now ready to define the graph feature extractor and its discriminatory ability.

Definition 4 (Graph feature extractor and its discriminatory ability)**.** *We say a mapping* Φ *is a graph feature extractor, if it maps a valued graph* $\mathrm{VALUE}_f(G)$ *to a new feature mapping* $\tilde{f}$ *on* G*. We further allow* Φ *to be parameterized as* Φ_θ*, and call* Φ_θ *a parameterized graph feature extractor.*

For a parameterized graph feature extractor Φ_θ*, we say* Φ_θ *has the discriminatory ability for* k*-neighbourhood sub-graphs, if for any valued graphs* (G, f) *and any two nodes* u, v *in* G*, if the valued* k*-neighbourhood sub-graph of* u *and* v *(i.e.,* $(G(u, k), f)$ *and* $(G(v, k), f)$*) are equivalent, there exists* $\theta^\star$ *such that* $\Phi_{\theta^\star}((G, f))(u) \neq \Phi_{\theta^\star}((G, f))(v)$*. In this case, we also say that* $\Phi_{\theta^\star}$ *can distinguish* u *and* v*.*

We point out that $\{h_i^{(l)}\}_i \cup \{h_{i,j}^{(l)}\}_{i,j}$ defined by Eqn. (2, 3, 4, 5) is a parameterized feature extractor, and thus above provides a formal definition of $\mathcal{O}$-GNN's discriminatory ability.

The next proposition shows that without the ring representation, the $\mathcal{O}$-GNN needs at least $k + 1$ layer to have the has the discriminatory power for k-neighbourhood sub-graphs.

Proposition 1. *Without the ring presentation,* $\mathcal{O}$*-GNN with no more than* k *layers does not have the discriminatory ability for* k*-neighbourhood sub-graphs.*

Note that Proposition 1 can be easily extended to the conventional graph convolutional neural networks, which only aggregate information from 1-neighborhood nodes. We then show that with the ring representations, $\mathcal{O}$-GNN with only one layer has the discriminatory power.

Proposition 2. *If* u *and* v *lie on different rings,* $\mathcal{O}$*-GNN with only one layer can distinguish them.*

The proofs are deferred to Appendix B due to space limitation. From Proposition 1 and 2, we can see that $\mathcal{O}$-GNN is more expressive than $\mathcal{O}$-GNN without rings. Without ring representations, the GNN requires at least k layers to distinguish two k-neighborhood nodes in a ring, while $\mathcal{O}$-GNN only requires one layer for this purpose.

4 EXPERIMENTS

To validate the effectiveness of our method, we test $\mathcal{O}$-GNN on the following three tasks: molecular property prediction, drug-drug interaction prediction and retrosynthesis. The first two tasks are graph classification tasks, and the third one is a node/link prediction task.

4.1 APPLICATION TO MOLECULAR PROPERTY PREDICTION

Datasets We work on three datasets for this application:

(1) The HOMO-LUMO energy gap prediction of the PCQM4Mv1 dataset (Hu et al., 2021). The input is a 2D molecular graph, and the target is its HOMO-LUMO energy gap, which is an essential molecular property in quantum chemistry. PCQM4Mv1 has 3045360 and 380670 training and validation data (test labels are not available). The properties are obtained via density function theory.

(2) Molecular property prediction on MoleculeNet dataset (Wu et al., 2018). This is a dataset about the prediction of pharmaceutical properties of small molecules. We choose six molecular property prediction tasks (including BBBP, Tox21, ClinTox, HIV, BACE and SIDER), and the data ranges from $1.5k$ to $41k$.

(3) Few-shot molecular property prediction of the FS-Mol dataset (Stanley et al., 2021). FS-Mol is made up of 5120 separate assays extracted from ChEMBL27 (`https://www.ebi.ac.uk/chembl/`). Each assay has 94 molecular-property pairs on average.

Method	MAE (↓)
GCN	0.1684
GCN + vn	0.1510
GIN	0.1536
GIN + vn	0.1396
ConfDSS	0.1278
Two-branch Transformer	0.1237
Graphormer$_{\text{base}}$	0.1193
Graphormer$_{\text{large}}$	0.1231
$\mathcal{O}$-GNN (ours)	0.1148

Table 1: Validation MAE on PCQM4Mv1.

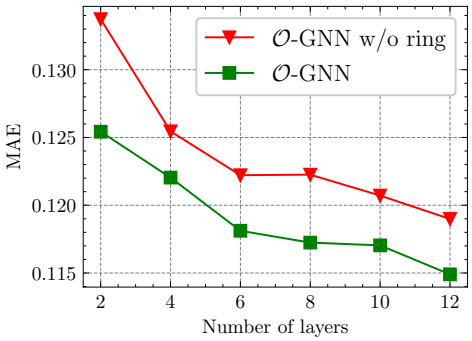

Figure 3: MAE w.r.t. numbers of layers.

Training configuration For PCQM4Mv1, we set the number of layers as 12 and hidden dimension as 256, which is selected by the cross-validation method on training set. For FS-Mol, the number of layers are 6 and the hidden dimension is 256. The candidate number of layers and hidden dimensions for MoleculeNet are $\{4, 6, 8, 12\}$ and $\{128, 256\}$. On FS-Mol and MoleculetNet, the hyperparameters are selected according to valiation performance. We train all these tasks on one GPU. The optimizer is AdamW (Loshchilov & Hutter, 2019). More detailed parameters are summarized in Table 5 of Appendix A.

Results on PCQM4Mv1 The results of PCQM4Mv1 are reported in Table 1. We compare $\mathcal{O}$-GNN with the following baselines: (1) Conventional GCN/GIN with/without virtual node (marked by "vn"). The results are from (Hu et al., 2021); (2) ConfDSS (Liu et al., 2021), which predicts quantum properties conditioned on low-cost conformer sets; (3) Two-branch Transformer (Xia et al., 2021), which has a regression head and a classification head that learning from each other; (4) Graphormer (Ying et al., 2021; Shi et al., 2022), the champion solution of PCQM4Mv1. Since the owners of PCQM4Mv1 did not release labels of the test set, we can only compare the results on the validation set. The evaluation metric is the mean absolute error (MAE). From Table 1, we can see that $\mathcal{O}$-GNN achieves the best results among the strong baseline models, which shows the effectiveness of our method. In addition, GIN vn, ConfDSS and Graphormer do not explicitly use the ring information, and we will combine $\mathcal{O}$-GNN with the strong methods in the future.

To investigate the significance of the ring information, we study a variant of $\mathcal{O}$-GNN by removing the ring modeling component from $\mathcal{O}$-GNN, and denote this variant as "$\mathcal{O}$-GNN w/o ring". Specifically, it is implemented by removing Eqn.(4) and all the h_r's in Eqn.(2,3,5). We conduct experiments for $\mathcal{O}$-GNN and "$\mathcal{O}$-GNN w/o ring" with 2, 4, 6, 8, 10 and 12 layers. The results are in Figure 3. We can see that by utilizing ring information, the performance is boosted regardless of the number of layers. In addition, we find that a 6-layer $\mathcal{O}$-GNN is comparable with the 12-layer $\mathcal{O}$-GNN w/o ring, which shows the great power of modeling rings in GNN.

Dataset # Molecules	BBBP 2039	Tox21 7831	ClinTox 1478	HIV 41127	BACE 1513	SIDER 1478
(Hu et al., 2020)	71.2 ± 0.9	74.2 ± 0.8	73.7 ± 4.0	75.8 ± 1.1	78.6 ± 1.4	60.4 ± 0.6
GROVER (Rong et al., 2020b)	70.3 ± 1.6	75.2 ± 0.3	77.8 ± 2.0	75.9 ± 0.9	79.2 ± 0.3	60.6 ± 1.1
GraphMVP (Liu et al., 2022)	72.4 ± 1.6	75.9 ± 0.5	79.1 ± 2.8	77.0 ± 1.2	81.2 ± 0.9	63.9 ± 1.2
GCN + vn	72.7 ± 1.3	75.0 ± 0.4	92.0 ± 1.1	78.8 ± 1.1	80.0 ± 0.8	62.9 ± 1.3
GIN + vn	71.7 ± 0.6	74.8 ± 0.6	89.4 ± 3.2	79.3 ± 1.0	82.0 ± 1.0	60.8 ± 0.8
$\mathcal{O}$-GNN w/o ring	74.5 ± 1.4	75.2 ± 0.9	90.2 ± 2.1	80.5 ± 1.0	84.2 ± 1.5	65.5 ± 1.6
$\mathcal{O}$-GNN (ours)	76.4 ± 0.4	75.7 ± 0.7	94.3 ± 1.6	81.3 ± 1.2	85.8 ± 1.0	66.2 ± 1.2

Table 2: Test ROC-AUC (%) performance of different methods on 6 binary classification tasks from MoleculeNet benchmark. The training, validation and test sets are provided by DeepChem in advance. Each experiment is independently run for three times. The mean and standard derivation are reported.

Results on MoleculeNet For MoleculeNet, we compare with both pretraining and non-pretraining methods. For non-pretraining methods, we compare with the following baselines: (i) GCN (Kipf & Welling, 2017) with virtual node ; (ii) GIN (Xu et al., 2018) with virtual node; (iii) $\mathcal{O}$-GNN without using ring information (denoted as "$\mathcal{O}$-GNN w/o ring"). For pre-training methods, we select several representative graph-based methods: (i) Hu et al. (2020) proposed to predict the masked attributes on graphs as well as maintaining the consistency between a subgraph and its neighbors; (ii) GROVER (Rong et al., 2020b) is a variant of Transformer for graphs and is pre-trained by prediction the properties of molecules in a self-supervised way. (iii) GraphMVP (Liu et al., 2022), which is a joint pre-training between 2D molecules and its 3D conformation. The results of (Hu et al., 2020), GROVER and GraphMVP are all extracted from Liu et al. (2022), since Liu et al. (2022) use the same scaffold-based splitting as us.

The results are reported in Table 2. We can see that: (i) $\mathcal{O}$-GNN outperforms the conventional network architectures like GIN and GCN with virtual nodes, which demonstrate the effectiveness of our new architecture; (ii) When comparing with the pre-training methods like GROVER (Rong et al., 2020b), GraphMVP (Liu et al., 2022) and Hu et al. (2020), $\mathcal{O}$-GNN still outperforms those methods. This shows the great potential of $\mathcal{O}$-GNN and we will combine it with pre-training in the future. (iii) Comparing $\mathcal{O}$-GNN and $\mathcal{O}$-GNN w/o ring, the average improvement overall the six tasks is 1.6. This shows the advantage of using ring information in molecular property prediction.

Results on FS-Mol Stanley et al. (2021) verify that prototypical networks (PN) performs the best on FS-Mol compared with other methods like MAML (Finn et al., 2017), multi-task learning and random forest. Stanley et al. (2021) use a Transformer-like residual network for few-shot classification. We replace that backbone to our $\mathcal{O}$-GNN, and the other parts remain unchanged. Following Stanley et al. (2021), the results with different support set sizes (denoted as $|\mathcal{T}_{u,support}|$) are reported. The evaluation metric is ΔAUPRC, which is the difference between the AUPRC (area under the precision-recall curve) and the ratio of the active compounds in that query set.

The results are in Figure 4. We have the following observations: (i) By using $\mathcal{O}$-GNN as the backbone model for the prototype network, the results are boosted for different support set sizes. (ii) The improvement is more significant when the support set size is large. When $|\mathcal{T}_{u,support}| = 128$ and 256, the improvements are 0.014 and 0.016. When reducing the sizes to 16/32/64, their improvements are all around 0.008. We will further improve the results on limited data size in the future.

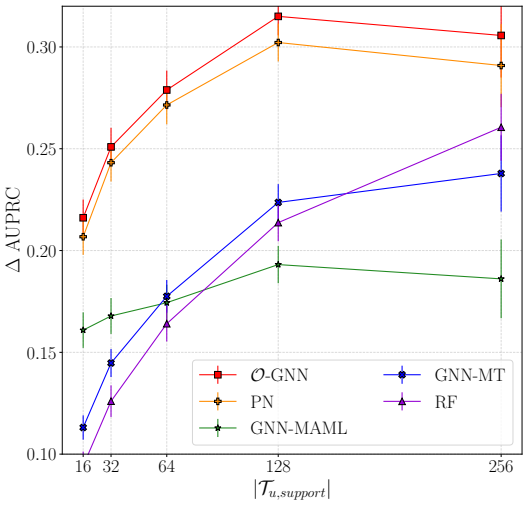

Figure 4: Results on FS-Mol. We report the mean and the standard derivations for different tasks across various support sizes.

4.2 Application to Drug-Drug Interaction Prediction

Drug-drug interaction prediction is to predict therapeutic output of taking two drugs together, like increasing the risk of some side effects, or it is effect enhanced to take them together. We focus on the classification task, where the inputs are two drug molecules and one interaction (e.g., inhibition), and the output is 0 or 1 to indicate whether the two drugs have this specific interaction. Following Nyamabo et al. (2022) and Li et al. (2022), we work on the inductive setting of the DrugBank dataset (Wishart et al., 2018), which has 1,706 drugs, 86 interaction types, and 191,808 triplets. To test the generalization ability of the model, we conduct experiments on two settings w.r.t. the drugs: the S1 setting, where neither of the two drugs on the test set appears in the training set; the S2 setting, where one drug is seen in the training set and the other is not. Noting that the drug pairs in the test set do not appear in the training set. Hence, the DrugBank data is split into training and test sets by the visibility

of the drugs, and the negative samples are offline generated. We directly use the data provided by Nyamabo et al. (2021; 2022), where 20% drugs are first hold as unseen drugs for formulating test set and the rest 80% drugs are used to create the training set.

Method	S2 setting (1 known drug + 1 unknown drug)				S1 setting (2 unknown drugs)			
	ACC	**AUROC**	**AP**	**F1**	**ACC**	**AUROC**	**AP**	**F1**
GAT-DDI (Nyamabo et al., 2021)	69.83	77.29	75.79	73.01	62.63	70.92	73.01	45.81
MHCADDI (Deac et al., 2019)	70.58	77.84	76.16	72.74	65.40	73.43	75.03	54.12
MR-GNN (Xu et al., 2019)	74.67	83.15	83.81	69.88	66.50	72.53	71.06	67.21
SSI-DDI (Nyamabo et al., 2021)	76.38	84.23	84.94	73.54	66.31	72.75	71.61	68.68
GMPNN (Nyamabo et al., 2022)	77.72	84.84	84.87	78.29	68.57	74.96	75.44	65.32
MSAN-GCN (Zhu et al., 2022)	77.81	85.74	–	76.48	69.17	76.12	–	67.10
MSN-DDI (Li et al., 2022)	81.92	91.01	91.09	80.18	73.42	81.79	81.82	70.34
$\mathcal{O}$-GNN (ours)	88.47	95.87	96.51	86.91	76.81	87.64	88.70	70.81

Table 3: Results of drug-drug interaction prediction on DrugBank.

To predict the interaction between two drugs, we use one 6-layer $\mathcal{O}$-GNN to extract features for the two drugs. Specifically, for each drug, we average the node representations output by the last layer as the drug feature. We concatenate the two drug features together, and then multiply the interaction embedding to do the prediction. The detailed parameters are left in Table 6 of Appendix A.

The results are reported in Table 3. $\mathcal{O}$-GNN significantly outperforms previous baselines in terms of accuracy (denoted as ACC), the area under the receiver operating characteristic (AUROC), the average precision (AP), and the F1 score. Most of previous works use GCN, GIN or GAT backbones, and they focus on designing comprehensive interaction module (Nyamabo et al., 2021; Li et al., 2022). By using the advanced $\mathcal{O}$-GNN backbone, we can significantly improve the results without designing complex interaction modules. This shows the effectiveness of our method.

4.3 Application to Retrosynthesis

Retrosynthesis is to predict the reactants of a given product. Various GNNs have been applied to this task. For example, GLN (Dai et al., 2019) use GNNs to predict the distributions of candidate reaction templates and reactants. GraphRetro (Somnath et al., 2021) and G2G (Shi et al., 2020) use GNNs to predict where to break a bond and how to add the fragments to complete the synthons. To demonstrate the ability of our $\mathcal{O}$-GNN, we combine our method with LocalRetro (Chen & Jung, 2021), the current best graph-based model for retrosynthesis (without using pre-training). LocalRetro uses GNN to predict the possible templates for each atom and each bond, and sort the predicted templates according to their probabilities. The top templates will be applied to the corresponding atoms or bonds via `RDKit` (Landrum et al., 2016) to generate the reactants. Chen & Jung (2021) use MPNN (Gilmer et al., 2017a) for prediction, and we replace the MPNN with $\mathcal{O}$-GNN.

We conduct experiments on the USPTO-$50k$ dataset (Coley et al., 2017) that contains $50,016$ reactions. Following Chen & Jung (2021), we partition the dataset as $45k$ training set, $5k$ validation set and $5k$ test set. The evaluation metric is the the top-k accuracy, where $k = 1, 3, 5, 10, 50$. The results are summarized in Table 4. We can observe that $\mathcal{O}$-GNN can predict reactions more accurately than the baselines without ring information. Especially, when the reaction type is known, we improve the top-1 accuracy for 1.8 points and the top-3 accuracy for 1.6 points. These results show the importance of modeling ring structure and the effectiveness of our method.

Method	Reaction type unknown					Reaction type known				
	Top-1	**Top-3**	**Top-5**	**Top-10**	**Top-50**	**Top-1**	**Top-3**	**Top-5**	**Top-10**	**Top-50**
G2G	48.9	67.6	72.5	75.5	–	61.0	81.3	86.0	88.7	–
GLN	52.5	69.0	75.6	83.7	92.4	64.2	79.1	85.2	90.0	93.2
GraphRetro	53.7	68.3	72.2	75.5	–	63.9	81.5	85.2	88.1	–
LocalRetro	53.4	77.5	85.9	92.4	97.7	63.9	86.1	92.4	96.3	97.9
$\mathcal{O}$-GNN (ours)	54.1	77.7	86.0	92.5	98.2	65.7	87.7	93.4	96.9	98.3

Table 4: Results on USPTO-$50k$ datasets with reaction type known/unknown.

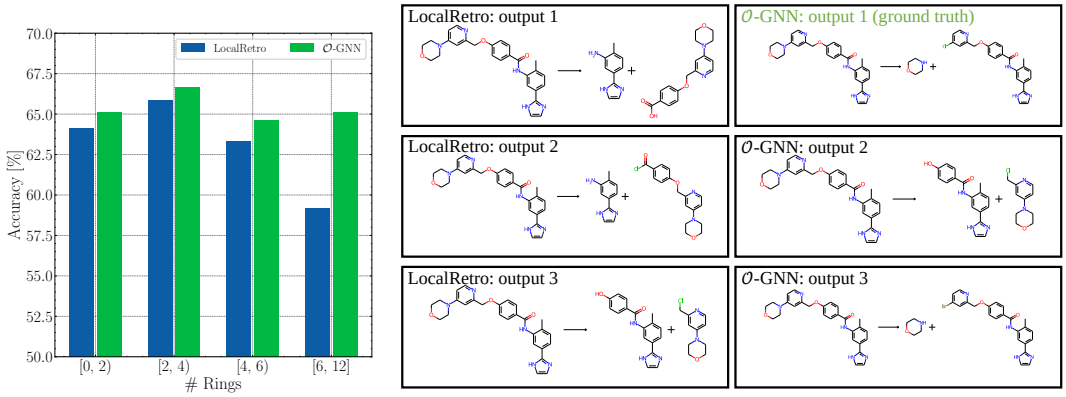

(a) Accuracy w.r.t #rings.

(b) Case study on molecule with complex rings.

Figure 5: Study of $\mathcal{O}$-GNN on retrosynthesis task. (a) The top-1 accuracy w.r.t. number of rings in product molecules. (b) The one-step retrosynthesis prediction of a product molecule with five rings. The left and right panels are the outputs of LocalRetro and $\mathcal{O}$-GNN. The groundtruth plan is the first one output by $\mathcal{O}$-GNN (marked as green).

The performance for different number of rings. To study the prediction performance of molecules with different number of rings, we group the USPTO-$50k$ test set by the number of rings in the product molecules and compute the top-1 accuracy for each group. More specifically, we divide the test set into four groups with ring numbers $[0, 2)$, $[2, 4)$, $[4, 6)$, $[6, 12]$, and those groups have 808, 2347, 1617, 235 reactions, respectively. The results are in Figure 5(a) where the blue bars represent the LocalRetro baseline and the green bars represent $\mathcal{O}$-GNN. The results show that $\mathcal{O}$-GNN has better accuracy on all groups, where the improvements are 0.99, 0.85, 1.30 and 5.96. Overall speaking, the improvement is larger when there are more rings in a molecule. Especially, when there are at least 6 rings in a group (i.e., the last column), $\mathcal{O}$-GNN increases the accuracy for 5.96 points, demonstrating that our method can better leverage ring structures.

Case study. In Figure 5(b), we show an example prediction of a product molecule with 5 rings. The reactions in the left panel are the top-3 predictions from LocalRetro baseline and the ones on the right are from $\mathcal{O}$-GNN. Our method successfully predicts the correct reactants in its first output (marked as green), but the baseline fails to give a correct prediction. More importantly, the baseline system even fails to identify the correct bond to change. These results suggest that modeling complex ring structures is crucial to predict reactions accurately, and $\mathcal{O}$-GNN is an effective algorithm for retrosynthesis.

5 Conclusions and Future Work

In this work, we propose a new model, ring-enhanced GNN (briefly, $\mathcal{O}$-GNN) for molecular modeling. We explicitly incorporate the ring representations into GNN and jointly update them with atom and bond representations. We provide theoretical analysis to $\mathcal{O}$-GNN and prove that by using $\mathcal{O}$-GNN, the node representations are more distinguishable than the variant without using ring representations. We conduct experiments on molecular property prediction, drug-drug interaction prediction and retrosynthesis. $\mathcal{O}$-GNN outperforms strong baselines on these tasks and achieves state-of-the-art results on the validation performance of PCQM4Mv1 and drug-drug interaction prediction. These results demonstrate the effectiveness of $\mathcal{O}$-GNN.

For future work, first, we will combine with pre-training to obtain a stronger $\mathcal{O}$-GNN. Second, we need to further improve our model when the training data is very limited (e.g., when the support set size is 16 or fewer). Third, how to efficiently identify and incorporate the representations with more complex structures is another interesting direction to explore. Fourth, we will apply our model to more real world scenarios, like the synthesis and generation of natural products with large rings.

REFERENCES

Gaurav Bhardwaj, Jacob O'Connor, Stephen Rettie, Yen-Hua Huang, Theresa A. Ramelot, Vikram Khipple Mulligan, Gizem Gokce Alpkilic, Jonathan Palmer, Asim K. Bera, Matthew J. Bick, Maddalena Di Piazza, Xinting Li, Parisa Hosseinzadeh, Timothy W. Craven, Roberto Tejero, Anna Lauko, Ryan Choi, Calina Glynn, Linlin Dong, Robert Griffin, Wesley C. van Voorhis, Jose Rodriguez, Lance Stewart, Gaetano T. Montelione, David Craik, and David Baker. Accurate de novo design of membrane-traversing macrocycles. *Cell*, 185(19):3520–3532.e26, 2022. ISSN 0092-8674. doi: https://doi.org/10.1016/j.cell.2022.07.019. URL https://www.sciencedirect.com/science/article/pii/S0092867422009229.

Shaked Brody, Uri Alon, and Eran Yahav. How attentive are graph attention networks? *arXiv preprint arXiv:2105.14491*, 2021.

Shuan Chen and Yousung Jung. Deep retrosynthetic reaction prediction using local reactivity and global attention. *JACS Au*, 1(10):1612–1620, 2021. doi: 10.1021/jacsau.1c00246.

Connor W. Coley, Luke Rogers, William H. Green, and Klavs F. Jensen. Computer-Assisted Retrosynthesis Based on Molecular Similarity. *ACS Central Science*, 3(12):1237–1245, December 2017. ISSN 2374-7943, 2374-7951. doi: 10.1021/acscentsci.7b00355. URL https://pubs.acs.org/doi/10.1021/acscentsci.7b00355.

Hanjun Dai, Chengtao Li, Connor Coley, Bo Dai, and Le Song. Retrosynthesis prediction with conditional graph logic network. In *Advances in Neural Information Processing Systems*, pp. 8870–8880, 2019.

Andreea Deac, Yu-Hsiang Huang, Petar Veličković, Pietro Liò, and Jian Tang. Drug-drug adverse effect prediction with graph co-attention. *arXiv preprint arXiv:1905.00534*, 2019.

Chelsea Finn, Pieter Abbeel, and Sergey Levine. Model-agnostic meta-learning for fast adaptation of deep networks. In Doina Precup and Yee Whye Teh (eds.), *Proceedings of the 34th International Conference on Machine Learning*, volume 70 of *Proceedings of Machine Learning Research*, pp. 1126–1135. PMLR, 06–11 Aug 2017.

Justin Gilmer, Samuel S. Schoenholz, Patrick F. Riley, Oriol Vinyals, and George E. Dahl. Neural message passing for quantum chemistry, 2017a. URL https://arxiv.org/abs/1704.01212.

Justin Gilmer, Samuel S Schoenholz, Patrick F Riley, Oriol Vinyals, and George E Dahl. Neural message passing for quantum chemistry. In *International conference on machine learning*, pp. 1263–1272. PMLR, 2017b.

Will Hamilton, Zhitao Ying, and Jure Leskovec. Inductive representation learning on large graphs. In I. Guyon, U. V. Luxburg, S. Bengio, H. Wallach, R. Fergus, S. Vishwanathan, and R. Garnett (eds.), *Advances in Neural Information Processing Systems*, volume 30. Curran Associates, Inc., 2017a. URL https://proceedings.neurips.cc/paper/2017/file/5dd9db5e033da9c6fb5ba83c7a7ebea9-Paper.pdf.

Will Hamilton, Zhitao Ying, and Jure Leskovec. Inductive representation learning on large graphs. *Advances in neural information processing systems*, 30, 2017b.

Weihua Hu, Bowen Liu, Joseph Gomes, Marinka Zitnik, Percy Liang, Vijay Pande, and Jure Leskovec. Strategies for pre-training graph neural networks. In *International Conference on Learning Representations*, 2020. URL https://openreview.net/forum?id=HJlWWJSFDH.

Weihua Hu, Matthias Fey, Hongyu Ren, Maho Nakata, Yuxiao Dong, and Jure Leskovec. Ogb-lsc: A large-scale challenge for machine learning on graphs. *arXiv preprint arXiv:2103.09430*, 2021.

Nirmala Chandralega Kampan, Mutsa Tatenda Madondo, Orla M McNally, Michael Quinn, and Magdalena Plebanski. Paclitaxel and its evolving role in the management of ovarian cancer. *Biomed Res. Int.*, 2015:413076, June 2015.

Sunghwan Kim, Jie Chen, Tiejun Cheng, Asta Gindulyte, Jia He, Siqian He, Qingliang Li, Benjamin A Shoemaker, Paul A Thiessen, Bo Yu, Leonid Zaslavsky, Jian Zhang, and Evan E Bolton. PubChem 2019 update: improved access to chemical data. *Nucleic Acids Res.*, 47(D1):D1102–D1109, January 2019.

Thomas N Kipf and Max Welling. Semi-supervised classification with graph convolutional networks. *ICLR*, 2017.

Greg Landrum et al. Rdkit: Open-source cheminformatics software, 2016. *URL http://www. rdkit. org/, https://github. com/rdkit/rdkit*, 149:150, 2016.

Junying Li, Deng Cai, and Xiaofei He. Learning graph-level representation for drug discovery. *arXiv preprint arXiv:1709.03741*, 2017.

Zimeng Li, Shichao Zhu, Bin Shao, Tie-Yan Liu, Xiangxiang Zeng, and Tong Wang. Multi-view substructure learning for drug-drug interaction prediction, 2022. URL https://arxiv.org/abs/2203.14513.

Meng Liu, Cong Fu, Xuan Zhang, Limei Wang, Yaochen Xie, Hao Yuan, Youzhi Luo, Zhao Xu, Shenglong Xu, and Shuiwang Ji. Fast quantum property prediction via deeper 2d and 3d graph networks, 2021. URL https://ogb.stanford.edu/paper/kddcup2021/pcqm4m_DIVE.pdf.

Shengchao Liu, Hanchen Wang, Weiyang Liu, Joan Lasenby, Hongyu Guo, and Jian Tang. Pre-training molecular graph representation with 3d geometry. In *International Conference on Learning Representations*, 2022. URL https://openreview.net/forum?id=xQUe1pOKPam.

Ilya Loshchilov and Frank Hutter. Decoupled weight decay regularization. In *International Conference on Learning Representations*, 2019. URL https://openreview.net/forum?id=Bkg6RiCqY7.

Andreas Loukas. What graph neural networks cannot learn: depth vs width. In *International Conference on Learning Representations*, 2020. URL https://openreview.net/forum?id=B1l2bp4YwS.

Arnold K Nyamabo, Hui Yu, and Jian-Yu Shi. Ssi–ddi: substructure–substructure interactions for drug–drug interaction prediction. *Briefings in Bioinformatics*, 2021.

Arnold K Nyamabo, Hui Yu, Zun Liu, and Jian-Yu Shi. Drug–drug interaction prediction with learnable size-adaptive molecular substructures. *Briefings in Bioinformatics*, 2022.

Trang Pham, Truyen Tran, Hoa Dam, and Svetha Venkatesh. Graph classification via deep learning with virtual nodes. *arXiv preprint arXiv:1708.04357*, 2017.

Yu Rong, Yatao Bian, Tingyang Xu, Weiyang Xie, Ying Wei, Wenbing Huang, and Junzhou Huang. Self-supervised graph transformer on large-scale molecular data. In *Proceedings of the 34th International Conference on Neural Information Processing Systems*, NIPS'20, Red Hook, NY, USA, 2020a. Curran Associates Inc. ISBN 9781713829546.

Yu Rong, Yatao Bian, Tingyang Xu, Weiyang Xie, Ying WEI, Wenbing Huang, and Junzhou Huang. Self-supervised graph transformer on large-scale molecular data. In H. Larochelle, M. Ranzato, R. Hadsell, M.F. Balcan, and H. Lin (eds.), *Advances in Neural Information Processing Systems*, volume 33, pp. 12559–12571. Curran Associates, Inc., 2020b. URL https://proceedings.neurips.cc/paper/2020/file/94aef38441efa3380a3bed3faf1f9d5d-Paper.pdf.

Sisi Shan, Shitong Luo, Ziqing Yang, Junxian Hong, Yufeng Su, Fan Ding, Lili Fu, Chenyu Li, Peng Chen, Jianzhu Ma, Xuanling Shi, Qi Zhang, Bonnie Berger, Linqi Zhang, and Jian Peng. Deep learning guided optimization of human antibody against sars-cov-2 variants with broad neutralization. *Proceedings of the National Academy of Sciences*, 119(11), 2022. doi: 10.1073/pnas.2122954119.

Chence Shi, Minkai Xu, Hongyu Guo, Ming Zhang, and Jian Tang. A graph to graphs framework for retrosynthesis prediction. In Hal Daumé III and Aarti Singh (eds.), *Proceedings of the 37th International Conference on Machine Learning*, volume 119 of *Proceedings of Machine Learning Research*, pp. 8818–8827. PMLR, 13–18 Jul 2020.

Yu Shi, Shuxin Zheng, Guolin Ke, Yifei Shen, Jiacheng You, Jiyan He, Shengjie Luo, Chang Liu, Di He, and Tie-Yan Liu. Benchmarking graphormer on large-scale molecular modeling datasets, 2022. URL https://arxiv.org/abs/2203.04810.

Vignesh Ram Somnath, Charlotte Bunne, Connor Coley, Andreas Krause, and Regina Barzilay. Learning graph models for retrosynthesis prediction. In M. Ranzato, A. Beygelzimer, Y. Dauphin, P.S. Liang, and J. Wortman Vaughan (eds.), *Advances in Neural Information Processing Systems*, volume 34, pp. 9405–9415. Curran Associates, Inc., 2021.

Megan Stanley, John F Bronskill, Krzysztof Maziarz, Hubert Misztela, Jessica Lanini, Marwin Segler, Nadine Schneider, and Marc Brockschmidt. FS-mol: A few-shot learning dataset of molecules. In *Thirty-fifth Conference on Neural Information Processing Systems Datasets and Benchmarks Track (Round 2)*, 2021. URL https://openreview.net/forum?id=701FtuyLlAd.

Jonathan M. Stokes, Kevin Yang, Kyle Swanson, Wengong Jin, Andres Cubillos-Ruiz, Nina M. Donghia, Craig R. MacNair, Shawn French, Lindsey A. Carfrae, Zohar Bloom-Ackermann, Victoria M. Tran, Anush Chiappino-Pepe, Ahmed H. Badran, Ian W. Andrews, Emma J. Chory, George M. Church, Eric D. Brown, Tommi S. Jaakkola, Regina Barzilay, and James J. Collins. A deep learning approach to antibiotic discovery. *Cell*, 180(4):688–702.e13, 2020. ISSN 0092-8674. doi: https://doi.org/10.1016/j.cell.2020.01.021. URL https://www.sciencedirect.com/science/article/pii/S0092867420301021.

Hongmao Sun, Gregory Tawa, and Anders Wallqvist. Classification of scaffold-hopping approaches. *Drug Discov. Today*, 17(7-8):310–324, April 2012.

Wen Torng and Russ B. Altman. Graph convolutional neural networks for predicting drug-target interactions. *Journal of Chemical Information and Modeling*, 59(10):4131–4149, 2019. doi: 10.1021/acs.jcim.9b00628.

Petar Veličković, Guillem Cucurull, Arantxa Casanova, Adriana Romero, Pietro Lio, and Yoshua Bengio. Graph attention networks. *arXiv preprint arXiv:1710.10903*, 2017.

Anilrudh A. Venugopal and Stuart Johnson. Fidaxomicin: A novel macrocyclic antibiotic approved for treatment of clostridium difficile infection. *Clinical Infectious Diseases*, 54(4):568–574, 12 2011. ISSN 1058-4838. doi: 10.1093/cid/cir830. URL https://doi.org/10.1093/cid/cir830.

David S Wishart, Yannick D Feunang, An C Guo, Elvis J Lo, Ana Marcu, Jason R Grant, Tanvir Sajed, Daniel Johnson, Carin Li, Zinat Sayeeda, et al. Drugbank 5.0: a major update to the drugbank database for 2018. *Nucleic acids research*, 46(D1):D1074–D1082, 2018.

Zhenqin Wu, Bharath Ramsundar, Evan N. Feinberg, Joseph Gomes, Caleb Geniesse, Aneesh S. Pappu, Karl Leswing, and Vijay Pande. Moleculenet: a benchmark for molecular machine learning. *Chemical Science*, 9:513–530, 2018. doi: 10.1039/C7SC02664A. URL http://dx.doi.org/10.1039/C7SC02664A.

Yingce Xia, Jinhua Zhu, Lijun Wu, Yang Fan, Shufang Xie, Yutai Hou, and Tao Qin. When transformer meets graph neural networks. 2021. URL https://ogb.stanford.edu/paper/kddcup2021/pcqm4m_GNNLearner.pdf.

Keyulu Xu, Weihua Hu, Jure Leskovec, and Stefanie Jegelka. How powerful are graph neural networks? *arXiv preprint arXiv:1810.00826*, 2018.

Nuo Xu, Pinghui Wang, Long Chen, Jing Tao, and Junzhou Zhao. Mr-gnn: Multi-resolution and dual graph neural network for predicting structured entity interactions. *arXiv preprint arXiv:1905.09558*, 2019.

Chengxuan Ying, Tianle Cai, Shengjie Luo, Shuxin Zheng, Guolin Ke, Di He, Yanming Shen, and Tie-Yan Liu. Do transformers really perform badly for graph representation? In *Advances in Neural Information Processing Systems*, volume 34, pp. 28877–28888, 2021.

Xinyu Zhu, Yongliang Shen, and Weiming Lu. Molecular substructure-aware network for drug-drug interaction prediction. *CIKM*, 2022.

A Detailed experiment configurations

The hyperparameters for the molecular property prediction, drug-drug interaction prediction and retrosynthesis are summarized in Table 5, Table 6 and Table 7 respectively.

	PCQM4Mv1	FS-Mol	MoleculeNet
Number of Layers	12	6	$\{4, 6, 8, 12\}$
Hidden dimension	256	256	$\{128, 256\}$
Optimizer	AdamW	AdamW	AdamW
Dropout	0.0	$\{0.0, 0.1, 0.2\}$	$\{0.0, 0.1, 0.2, 0.3, 0.5\}$
Learning rate	0.0003	$\{0.0001, 0.0002, 0.0003\}$	{0.00005,0.0001,0.0002,0.0005}
Training steps	300 epochs	10000 iterations	{50,100} epochs
Batch size	512	16	{32,64}
Weight Decay	0.1	$\{0.01, 0.1\}$	0.01
Learning Rate Decay	Cosine	Cosine	Linear

Table 5: Detailed hyper-parameters for molecular property prediction tasks.

Number of Layers	6
Hidden dimension	512
Optimizer	AdamW
Dropout	$\{0.2, 0.5\}$
Learning rate	0.0003
Training steps	100 epochs
Batch size	128
Weight Decay	0.01
Learning Rate Decay	Cosine

Table 6: Detailed hyper-parameters for drug-drug interaction prediction.

Number of Layers	6
Hidden dimension	512
Optimizer	AdamW
Dropout	0.1
Learning rate	0.0003
Training steps	200 epochs
Batch size	64
Weight Decay	0.1
Learning Rate Decay	Cosine

Table 7: Detailed hyper-parameters for retrosynthesis.

B Proofs of the two propositions

Proof of Proposition 1. We start the proof by explicitly writing down the ring-free variant of $\mathcal{O}$-GNN.

Specifically, the bond representations are given by

$$h_{ij}^{(l)} = h_{ij}^{(l-1)} + \texttt{MLP}(h_i^{(l-1)}, h_j^{(l-1)}, h_{ij}^{(l-1)}, U^{(l-1)}).$$

The atom representations are given by

$$\begin{aligned}
&\bar{h}_i^{(l)} = \sum_{j\in\mathcal{N}(i)} \alpha_j W_v \texttt{concat}(h_{ij}^{(l)}, h_j^{(l-1)});\\
&\alpha_j \propto \exp(\boldsymbol{a}^\top \texttt{LeakyReLU}(W_q h_i^{(l-1)} + W_k \texttt{concat}(h_j^{(l-1)}, h_{ij}^{(l)})));\\
&h_i^{(l)} = h_i^{(l-1)} + \texttt{MLP}\Big(h_i^{(l-1)}, \bar{h}_i^{(l)}, U^{(l-1)}\Big).
\end{aligned} \tag{6}$$

The compound representations are given by

$$U^{(l)} = U^{(l-1)} + \texttt{MLP}\left(\frac{1}{|V|}\sum_{i=1}^{|V|} h_i^{(l)}, \frac{1}{|E|}\sum_{i,j} h_{ij}^{(l)}, U^{(l-1)}\right). \tag{7}$$

Given the above notations, Proposition 1 can then be translated to the following claim:

Claim. For any valued graphs (G, f) and any two nodes v_a, v_b in G, if the valued k-neighbourhood sub-graph of u and v (i.e., $(G(v_a, k), f)$ and $(G(v_b, k), f)$) are equivalent, we have that $h_a^l = h_b^l$ for any $l \in \{1, \cdots, k\}$ holds regardless of the parameter.

We denote the equivalent mapping between $(G(v_a, k), f)$ and $(G(v_b, k), f)$ as $\mathcal{P}$. We will slightly abuse the notations by letting $\mathcal{P}(i) = j$ if $\mathcal{P}(v_i) = v_j$.

We will prove the above claim by induction. Specifically, we will prove that for any $l \in \{0, 1, \cdots, k\}$, we have $h_{c_1}^l = h_{\mathcal{P}(c_1)}^l$ for any $v_{c_1} \in V(v_a, k-l)$, and $h_{c_1c_2}^l = h_{\mathcal{P}(c_1)\mathcal{P}(c_2)}^l$ for any $v_{c_1}, v_{c_2} \in V(v_a, k-l)$.

Base case: for $l = 0$, by the definition of f, we have $f(v_{c_1}) = f(\mathcal{P}(v_{c_1}))$ for every $v_{c_1} \in V(v_a, k)$ and $f(v_{c_1}, v_{c_2}) = f(\mathcal{P}(v_{c_1}), \mathcal{P}(v_{c_2}))$ for every $v_{c_1}, v_{c_2} \in V(v_a, k)$. The claim immediately follows as $h_{c_1}^0 = f(v_{c_1})$, $h_{\mathcal{P}(c_1)}^0 = f(\mathcal{P}(v_{c_1}))$, $h_{c_1c_2}^0 = f(v_{c_1}, v_{c_2})$, and $h_{\mathcal{P}(c_1)\mathcal{P}(c_2)}^0 = f(\mathcal{P}(c_1), \mathcal{P}(c_2))$.

Induction step: suppose the claim is true for $l = i \in \{0, \cdots, k-1\}$. Then, for $l = i+1$, we have that for every $v_{c_1}, v_{c_2} \in V(v_a, k-l)$,

$$\begin{aligned}
h_{c_1c_2}^{(l)} =& h_{c_1c_2}^{(l-1)} + \texttt{MLP}(h_{c_1}^{(l-1)}, h_{c_2}^{(l-1)}, h_{c_1c_2}^{(l-1)}, U^{(l-1)})\\
\overset{(\star)}{=}& h_{\mathcal{P}(c_1)\mathcal{P}(c_2)}^{(l-1)} + \texttt{MLP}(h_{\mathcal{P}(c_1)}^{(l-1)}, h_{\mathcal{P}(c_2)}^{(l-1)}, h_{\mathcal{P}(c_1)\mathcal{P}(c_2)}^{(l-1)}, U^{(l-1)})\\
=& h_{\mathcal{P}(c_1)\mathcal{P}(c_2)}^{(l)},
\end{aligned} \tag{8}$$

where $Eq.(\star)$ is due to the induction hypothesis, as $v_{c_1}, v_{c_2} \in V(v_a, k-l) \subset V(v_a, k-(l-1))$.

Similarly, for every $v_{c_1} \in V(v_a, k-l)$,

$$\begin{aligned}
\bar{h}_{c_1}^{(l)} =& \sum_{j\in\mathcal{N}(c_1)} \alpha_j W_v \texttt{concat}(h_{c_1j}^{(l)}, h_j^{(l-1)})\\
\overset{(\circ)}{=}& \sum_{j\in\mathcal{N}(c_1)} \alpha_j W_v \texttt{concat}(h_{\mathcal{P}(c_1)\mathcal{P}(j)}^{(l)}, h_{\mathcal{P}(j)}^{(l-1)})\\
\overset{(\diamond)}{=}& \sum_{j\in\mathcal{N}(c_1)} \alpha_{\mathcal{P}(j)} W_v \texttt{concat}(h_{\mathcal{P}(c_1)\mathcal{P}(j)}^{(l)}, h_{\mathcal{P}(j)}^{(l-1)})\\
=& \sum_{j\in\mathcal{N}(c_1)} \alpha_j W_v \texttt{concat}(h_{\mathcal{P}(c_1)j}^{(l)}, h_j^{(l-1)})\\
=& \bar{h}_{\mathcal{P}(c_1)}^{(l)},
\end{aligned}$$

where Eq. $(\circ)$ is due to the induction hypothesis and Eq. (8). Eq. $(\diamond)$ is due to

$$\begin{aligned}
\alpha_j \propto& \exp(\boldsymbol{a}^\top \texttt{LeakyReLU}(W_q h_{c_1}^{(l-1)} + W_k \texttt{concat}(h_j^{(l-1)}, h_{c_1j}^{(l)})))\\
=& \exp(\boldsymbol{a}^\top \texttt{LeakyReLU}(W_q h_{\mathcal{P}(c_1)}^{(l-1)} + W_k \texttt{concat}(h_{\mathcal{P}(j)}^{(l-1)}, h_{\mathcal{P}(c_1)\mathcal{P}(j)}^{(l)}))),
\end{aligned}$$

and thus $\alpha_j = \alpha_{\mathcal{P}(j)}$ for any $j \in \mathcal{N}(c_1)$.

We then have

$$\begin{aligned} h_{c_1}^{(l)} =& h_{c_1}^{(l-1)} + \texttt{MLP}\Big(h_{c_1}^{(l-1)}, \bar{h}_{c_1}^{(l)}, U^{(l-1)}\Big) \\ =& h_{\mathcal{P}(c_1)}^{(l-1)} + \texttt{MLP}\Big(h_{\mathcal{P}(c_1)}^{(l-1)}, \bar{h}_{\mathcal{P}(c_1)}^{(l)}, U^{(l-1)}\Big) \\ =& h_{\mathcal{P}(c_1)}^{(l)}. \end{aligned}$$

Thus, the claim holds for $l = i+1$, and the proof for the induction claim completes. Thus, the claim is true for every $l \in \{0, \cdots, k\}$.

For every $l \in \{0, \cdots, k\}$ $u \in G(v_a, 0) \subset G(v_a, k-l)$. Therefore, we have $h_a^{(l)} = h_{\mathcal{P}(a)}^{(l)} = h_b^{(l)}$, and the proof is completed. □

Proof of Proposition 2. For two equivalent valued sub-graph $(G(v_a, k), f)$ and $(G(v_b, k), f)$, if v_a and v_b lie on different rings, we have

$$\frac{1}{|R(v_a)|} \sum_{r \in R(v_a)} h_r^{(0)} \neq \frac{1}{|R(v_b)|} \sum_{r \in R(v_b)} h_r^{(0)}.$$

Therefore, there exists a choice of MLP, such that

$$\begin{aligned} h_a^{(1)} =& h_a^{(0)} + \texttt{MLP}\Big(h_a^{(0)}, \bar{h}_a^{(1)}, \frac{1}{|R(v_a)|} \sum_{r \in R(v_a)} h_r^{(0)}, U^{(0)}\Big) \\ \neq& h_b^{(0)} + \texttt{MLP}\Big(h_b^{(0)}, \bar{h}_b^{(1)}, \frac{1}{|R(v_b)|} \sum_{r \in R(v_b)} h_r^{(0)}, U^{(0)}\Big) \\ =& h_b^{(1)}. \end{aligned}$$

The proof is completed. □